

Electrical enhancement period of solar photovoltaic using phase change material

Sourav Khanna^{a,*}, Sanjeev Newar^b, Vashi Sharma^c, K. S. Reddy^d, Tapas K. Mallick^{e,*}, Jovana Radulovic^f, Rinat Khusainov^g, David Hutchinson^h, Victor Becerra^a

^aSchool of Energy and Electronic Engineering, University of Portsmouth, Portsmouth PO1 3DJ, United Kingdom

^bDepartment of Industrial and Management Engineering, IIT Kanpur, India

^cDepartment of Mechanical Engineering, IIT Kanpur, India

^dDepartment of Mechanical Engineering, IIT Madras, India

^eEnvironment and Sustainability Institute, Penryn Campus, University of Exeter, United Kingdom

^fSchool of Mechanical and Design Engineering, University of Portsmouth, Portsmouth PO1 3DJ, United Kingdom

^gSchool of Computing, University of Portsmouth, Portsmouth PO1 3DJ, United Kingdom

^hFaculty of Technology, University of Portsmouth, Portsmouth PO1 3AH, United Kingdom

Abstract

Temperature management in photovoltaic (PV) is critical for the power output. Phase Change Material (PCM) usage enables one to remove heat from the system and achieve enhanced electrical output. This study aims at finding the period of PV electrical enhancement, the increase in power and increase in electrical efficiency achieved using PCM under different working circumstances. Results suggest that as the angle of approach of wind changes from 75° to 0°, the electrical enhancement period elevates from 7.0 h to 8.6 h for 5 cm deep PCM box. But, the increase in power drops from 17.6 W/m² to 13.6 W/m². As wind speed changes from 6 m/s to 0.2 m/s, the electrical enhancement period drops from 9.1 h to 6.4 h. But, the increase in power rises from 11.8 W/m² to 22.8 W/m². The rise in ambient temperature 289 K to 299 K leads to decrement of electrical enhancement period from 12.6 h to 7.1 h. But the increase in power rises from 15.9 W/m² to 21.4 W/m². Elevation in temperature for liquification from 291 K to 301 K leads to increment of electrical enhancement period from 6.5 h to 12.3 h.

* Corresponding Authors

Email: sourav.khanna@port.ac.uk (Sourav Khanna)

t.k.mallick@exeter.ac.uk (Tapas K. Mallick)

29 **1. Introduction**

30 **1.1 Motivation**

31 Temperature management in photovoltaic is critical for the power output. Phase Change
32 Material usage enables one to remove heat from the system and achieve enhanced electrical
33 output.

34 **1.2 Literature Review**

35 Experiments have been performed on PV in Tehran using PCM by Baygi and Sadrameli (2018).
36 The setup witnesses the PV temperature drop of 15°C against the case of no PCM where the
37 temperature rises till 60°C. The impact of different climates of Vehari and Dublin using PCM
38 discussed by Hasan et al. (2015). The respective PV temperature drops attained in two cases
39 are reported as 21.5°C and 10°C. Experiments on a virtual PV with paraffin wax as coolant
40 have been reported by Huang et al. (2006, 2007). It has also been concluded that the fins in the
41 PCM can cause even more cooling. Lu et al. (2018) have also analysed the fins in the PCM for
42 the cooling of building integrated concentrating photovoltaic and found a 12% improvement in
43 electrical efficiency. Comparison between two different setups has been carried out by
44 Indartono et al. (2014) for Indonesia. Same PCM is filled on back sides of a) PV inclined at a
45 support, and b) PV placed in touch with roof. The respective cooling is reported as 2.6°C and
46 5.7°C. Hasan et al. (2010) have compared PCMs amongst a range for their performances in
47 terms of cooling. The authors have reported the highest cooling of 18°C in case of PCMs: CP-
48 acid and $\text{CaCl}_2\text{H}_{12}\text{O}_6$. Kamkari and Groulx (2018) have discussed the dynamics of lauric acid-
49 PCM during melting when heated from rear. The melting rate of PCM is found to be fastest
50 when box is kept grounded rather than standing or slanted. Zhang et al. (2018) have reported a
51 review study on the use of solid-liquid PCM for the thermal energy storage. An innovative kind
52 of PCM, infused with nano-particles is studied by Sharma et al. (2017). Waqas et al. (2017)

53 have equipped the PV with PCM filled metallic tubes. Indian state of Punjab has been chosen
54 by Preet et al. (2017) to carry out experimental study using paraffin wax 30 as PCM. The PV
55 temperature has been recorded to have come down by an effective 25°C. Browne et al. (2015,
56 2016) have performed experiments with a differently synthesised compound constituting
57 various materials that are chemically inert to each other. Different fatty acids are used to form
58 the desired PCM that have caused temperature drop of 5.5°C. Tracking setups with paraffin
59 wax as PCM have been experimentally monitored by Su et al. (2018) in Macau and an effective
60 enhancement of 10% in electrical output has been achieved. Siyabi et al. (2018a, 2018b) have
61 used multiple PCM heat sink and stacked heat sink for the purpose of thermal management.

62 Brano et al. (2014) have simultaneously studied the impact of time and space using forward and
63 central difference models respectively using paraffin wax 27 as PCM. The approach is used to
64 compare computational and experimental results. The comparison testifies correctness of the
65 approach as the difference does not exceed -6.5°C and 7.5°C on either side. Kant et al. (2016)
66 have studied the paraffin wax 35 PCM using conduction-alone model and conduction-
67 convection model. The respective PV cooling is reported as 1.5°C and 5°C. Graphite with
68 permeating PCM is used by Atkin and Farid (2015) and an improvement of 7% is observed in
69 power output. Implicit method to model enthalpy has been applied by Kibria et al. (2016) for
70 comparing variants of paraffin wax viz. 20, 25, and 28. Paraffin wax 20 is found to have
71 liquefied at fastest rate among all three. Ma et al. (2018) have performed the sensitivity analysis
72 of PV-PCM system. Benlekkam et al. (2018) have studied the impact of tilt of fins on the
73 performance of PV-PCM. Biwole et al. (2013, 2018) have studied the PCM domain with
74 suitable modelling by emphasizing on the elimination of the cases leading to divergence. The
75 optimum values for the liquification temperature of PCM have been reported for PV-PCM and
76 PVT-PCM systems by Park et al. (2014) and Su et al. (2017) respectively. Khanna et al. (2018a,
77 2018b) have investigated the impact of climates on the contribution of PCM in PV cooling and

78 carried out the optimization (Khanna et al., 2018c; 2018d; 2019). Arici et al. (2018) have also
79 carried out the optimization of PV-PCM system. Khanna et al. (2018e) have studied PV-PCM
80 system for Cornwall. Various alignments of heat-exchangers transferring heat to PCM are
81 investigated by Emam and Ahmed (2018) and parallel alignment is reported as best.
82 Computational results for a virtual PV with paraffin wax as coolant have been reported by
83 Huang et al. (2004, 2011). It has been concluded that the fins in the PCM can cause further
84 cooling. Emam et al. (2017) and Khanna et al. (2017a) have investigated CPV-PCM and PV-
85 PCM when heated from front. The PCM's melting rate was found to be fastest when box was
86 kept standing or slanted rather than grounded. The adoption of analytical expressions (Khanna
87 et al., 2014; 2016; Khanna and Sharma, 2015; 2016; Sharma et al. 2016) can ease the
88 calculations in the domain of PV-PCM thermal analysis. Sathe and Dhoble (2018) have used
89 extended surfaces in the PCM to enhance the cooling of CPV.

90 **1.3 Contribution**

91 In the current work, the period of PV electrical enhancement, the increase in power and increase
92 in electrical efficiency achieved using PCM under different working circumstances are
93 reported.

94 **2. Physical Model**

95 PV and PV-PCM having an inclination angle of β are considered (Fig. 1). Dimensions of PCM
96 box are L and d respectively.

97 The presented study is applicable within the following suppositions

- 98 (i) Solar energy density is similar over the surface of PV
- 99 (ii) Outer surfaces of PCM box are kept thermally isolated from ambient
- 100 (iii) Properties of PV, solidus PCM and liquidus PCM are unaltered across directions
101 and space

102 (iv) PV is constructed by coupling 5 different coverings and thermal resistances in
 103 between the coverings are neglected

104 3. Mathematical Modelling

105 The solar irradiance soaked up by PV that does not take part in electricity generation leads to
 106 thermal energy production. It has been articulated as

$$107 \quad E = \left[(\tau\alpha)_c S - \eta_{STC} S \left\{ 1 + \beta_c (T_{PV} - 25) + \gamma_c \ln \left(\frac{S}{1000} \right) \right\} \right] / t_{si} \quad (1)$$

108 The initial term of the aforementioned equation covers the solar irradiance soaked up by PV
 109 and latter term covers the power production that takes into account the impact of PV
 110 temperature and intensity of solar irradiance. A part of the thermal energy dissipates radiatively
 111 and convectively from the top and back. Forced part of convective mode is articulated by taking
 112 into account the impact of wind speed (s_w) and angle of approach of wind (γ_w) for top (h_t) and
 113 back (h_b) as (Kaplani and Kaplanis, 2014)

$$114 \quad h_t = 0.848 k_a [\sin \beta \cos \gamma_w s_w Pr / \nu]^{1/2} (L_{ch}/2)^{-1/2} \quad (2)$$

$$115 \quad h_b = \begin{cases} 3.83 s_w^{0.5} L_{ch}^{-0.5} & \text{for laminar flow} \\ 5.74 s_w^{0.8} L_{ch}^{-0.2} - 16.46 L_{ch}^{-1} & \text{for mixed flow} \\ 5.74 s_w^{0.8} L_{ch}^{-0.2} & \text{for fully turbulent flow} \end{cases} \quad (3)$$

116 Natural part of convective mode is articulated by using Nusselt number for top (Nu_t) and back
 117 (Nu_b) as (Kaplani and Kaplanis, 2014; Khanna et al., 2017)

$$118 \quad Nu_t = \begin{cases} [0.13(PrGr)^{0.33}] & \text{for } \beta \leq 30^\circ \\ [0.13\{(PrGr)^{0.33} - (PrGr_c)^{0.33}\} + 0.56(PrGr_c \sin \beta)^{0.25}] & \text{for } \beta > 30^\circ \end{cases} \quad (4)$$

$$119 \quad Nu_b = \begin{cases} 0.58(Ra)^{0.2}; & \text{for } \beta \leq 2^\circ \\ 0.56(Ra \sin \beta)^{0.25}; & \text{for } 2^\circ < \beta < 30^\circ \\ \left[0.825 + \frac{0.387(Ra \sin \beta)^{0.1667}}{\{1 + (0.492/Pr)^{0.5625}\}^{0.2963}} \right]^2 & \text{for } \beta \geq 30^\circ \end{cases} \quad (5)$$

120 3.1 Solid Components

121 The energy balance for the i^{th} layer of the solid components can be written as

$$122 \quad \rho_i C_{p,i} \frac{\partial T_i}{\partial t} = \nabla \cdot (k_i \nabla T_i) + E_i \quad (6)$$

123 with below boundaries

$$124 \quad k_i \frac{\partial T_i}{\partial y} = h_c [T_i - T_a] + F_{t_sk} \sigma \varepsilon_t [T_t^4 - T_{sk}^4] + F_{t_gr} \sigma \varepsilon_t [T_t^4 - T_{gr}^4] \quad \text{at top} \quad (7)$$

$$125 \quad k_i \frac{\partial T_i}{\partial x} = 0 \quad \text{at edges} \quad (8)$$

$$126 \quad k_i \frac{\partial T_i}{\partial y} = k_{i+1} \frac{\partial T_{i+1}}{\partial y} \quad \text{at interface} \quad (9)$$

$$127 \quad k_i \frac{\partial T_i}{\partial y} = h_c [T_i - T_a] + F_{re_sk} \sigma \varepsilon_{re} [T_i^4 - T_{sk}^4] + F_{re_gr} \sigma \varepsilon_{re} [T_i^4 - T_{gr}^4] \quad \text{at rear} \quad (10)$$

$$128 \quad T_i = T_a \quad \text{when } t = 0 \quad (11)$$

129 Eq. (7) covers the convective energy loss from top to the ambient, radiative energy loss from
 130 top to the sky and from top to ground. Both forced (Eq. 2) and natural (Eq. 4) modes of
 131 convective energy flow are considered. Eq. (8) covers no heat loss condition at the edges.

132 3.2 Phase Change Material

133 The energy/momentum/mass balances for the PCM can be written as

$$134 \quad \rho_P C_p \frac{\partial T_P}{\partial t} = \nabla \cdot (k_P \nabla T_P) - \rho_P C_{p,P} (\vec{v} \cdot \nabla T_P) \quad (12)$$

$$135 \quad \rho_P \frac{\partial v_x}{\partial t} + \rho_P v_x \frac{\partial v_x}{\partial x} + \rho_P v_y \frac{\partial v_x}{\partial y} = -\frac{\partial p}{\partial x} + \mu_{P,l} \nabla^2 \vec{v} + \rho_{P,l} g_x [1 - \beta_c (T_P - T_m)] - F_x \quad (13)$$

$$136 \quad \rho_P \frac{\partial v_y}{\partial t} + \rho_P v_x \frac{\partial v_y}{\partial x} + \rho_P v_y \frac{\partial v_y}{\partial y} = -\frac{\partial p}{\partial y} + \mu_{P,l} \nabla^2 \vec{v} + \rho_{P,l} g_y [1 - \beta_c (T_P - T_m)] - F_y \quad (14)$$

$$137 \quad \nabla \cdot \vec{v} = 0 \quad (15)$$

138 with below boundaries

139 $k_P \frac{\partial T_P}{\partial y} = k_{al} \frac{\partial T_{al}}{\partial y}$ for aluminium – PCM interface along length (16)

140 $k_P \frac{\partial T_P}{\partial x} = k_{al} \frac{\partial T_{al}}{\partial x}$ for aluminium – PCM interface along depth (17)

141 $T_P = T_a$ when $t = 0$ (18)

142 $v_x = v_y = 0$ at inner surface of PCM box (19)

143 $v_x = v_y = 0$ when $t = 0$ (20)

144 ANSYS Fluent 17.1 is used to solve the above equations.

145 **4. Experimental Validation**

146 Experimentations to study the photovoltaic with phase change material are carried out (Hasan
147 et al., 2015). To establish the precision of the current model by comparing the computed results
148 with experimental observations, the analysis is carried out using same system. The computed
149 values of the average PV temperature are put against the experimental observations in Figure
150 2. The results suggest that the both match satisfactorily.

151 **5. Results and Discussion**

152 The period of electrical enhancement, power production, electrical efficiency, increase in
153 electrical efficiency and increase in power have been computed. The specifications are
154 presented by Khanna et al. (2019).

155 **5.1 Period of Electrical Enhancement and Increase in Power**

156 **5.1.1 Impact of Wind Speed**

157 The period of electrical enhancement of PV has been computed for a span of wind speed and
158 deepness of PCM box and plotted in Figure 3. The results show that as wind speed drops from
159 6 m/s to 5 m/s, 4 m/s, 3 m/s, 2 m/s, 1 m/s and 0.2 m/s, the electrical enhancement period
160 decreases from 9.1 h to 8.8 h, 8.5 h, 8.0 h, 7.5 h, 6.9 h and 6.4 h respectively for 5cm deep PCM
161 box. The reason can be explained as follows. The low wind speed drops the thermal loss and
162 increases the heat collection rate by PCM that increases the speed of liquification and, thus,
163 drops the period of electrical enhancement.

164 The electricity generation and electrical efficiency have been computed for a span of wind speed
165 and plotted in Figures 4 and 5. The results show that as wind speed drops from 6 m/s to 5 m/s,
166 4 m/s, 3 m/s, 2 m/s, 1 m/s and 0.2 m/s, the electricity generation decreases from 191.3 to 191.0,
167 190.4, 189.6, 188.5, 187.0 and 185.4 W/m² respectively. The reason can be explained as
168 follows. The low wind speed decreases the heat losses from the PV which leads to increase in
169 the PV temperature resulting in decrease in the electricity generation.

170 The increase in power and electrical efficiency achieved by PCM have been computed for a
171 span of wind speed and plotted in Figures 4 and 5. The results show that as wind speed drops
172 from 6 m/s to 5 m/s, 4 m/s, 3 m/s, 2 m/s, 1 m/s and 0.2 m/s, the increase in power elevates from
173 11.8 to 12.4, 13.6, 15.0, 17.0, 19.8 and 22.8 W/m² respectively. The reason can be explained as
174 follows. The high wind speed takes away the PV's heat efficiently and cools the PV which
175 decreases the contribution of phase change material in PV cooling.

176 **5.1.2 Impact of Angle of Approach of Wind**

177 The period of electrical enhancement of PV has been computed for a span of angle of approach
178 of wind and deepness of PCM box and plotted in Figure 6. The results show that as the angle
179 of approach of wind decreases from 75° to 60°, 45°, 30°, 15° and 0°, the electrical enhancement
180 period increases from 7.0 h to 7.6 h, 8.0 h, 8.3 h, 8.5 h and 8.6 h for 5 cm deep PCM box. The
181 reason can be explained as follows. When wind approaches normally to PV, it takes away the
182 PV's heat efficiently that reduces the rate of heat collection by PCM and reduces the speed of
183 liquification and, thus, increases the period of electrical enhancement.

184 The electricity generation and electrical efficiency have been computed for a span of angle of
185 approach of wind and plotted in Figures 7 and 8. The results show that as the angle of approach
186 of wind decreases from 75° to 60°, 45°, 30°, 15° and 0°, the electricity generation increases
187 from 189.2 to 189.7, 190.0, 190.2, 190.3 and 190.4 W/m² respectively. The reason can be
188 explained as follows. When wind approaches normally to PV, it takes away the PV's heat
189 efficiently which leads to decrease in the PV temperature resulting in increase in the electricity
190 generation and the electrical efficiency.

191 The increase in power and electrical efficiency achieved using PCM have been computed for a
192 span of angle of approach of wind and plotted in Figures 7 and 8. The results show that as the
193 angle of approach of wind decreases from 75° to 60°, 45°, 30°, 15° and 0°, the increase in power
194 reduces from 17.6 to 15.9, 14.8, 14.1, 13.7 and 13.6 W/m² respectively. It is because the low
195 wind azimuth angle increases the heat losses from the PV and cools the PV which decreases
196 the contribution of phase change material in PV cooling.

197 **5.1.3 Impact of Surroundings Temperature**

198 The period of electrical enhancement of PV has been computed for a span of surroundings
199 temperature and deepness of PCM box and plotted in Figure 9. The results show that as the
200 surroundings temperature increases from 289 K to 291 K, 293 K, 295 K, 297 K and 299 K, the
201 electrical enhancement period drops from 12.6 h to 10.9 h, 9.6h, 8.6 h, 7.7 h and 7.1 h
202 respectively for 5 cm deep PCM box. The reason can be explained as follows. For the case of
203 higher surrounding temperature, the rate of heat collection by PCM rises that increases the
204 speed of liquification and, thus, drops the period of electrical enhancement.

205 The electricity generation and electrical efficiency have been computed for a span of
206 surroundings temperature and plotted in Figures 10 and 11. The results show that as the
207 surroundings temperature increases from 289 K to 291 K, 293 K, 295 K, 297 K and 299 K, the
208 electrical generation drops from 194.8, 192.8, 190.9, 188.9, 186.9 and 185.0 W/m². It is because
209 for the case of higher surrounding temperature, the PV temperature rises which leads to
210 decrease in the electricity generation and electrical efficiency.

211 The increase in power and electrical efficiency achieved using PCM have been computed for a
212 span of surroundings temperature and plotted in Figures 10 and 11. The results show that as
213 surroundings temperature increases from 289 K to 291 K, 293 K, 295 K, 297 K and 299 K, the
214 increase in power elevates from 15.9 to 17.0, 18.1, 19.2, 20.3 and 21.4 W/m² respectively. It is
215 because the low surrounding temperature keeps the PV operating temperature low which
216 decreases the contribution of phase change material in PV cooling.

217 **5.1.4 Impact of PCM Liquification Temperature**

218 The period of electrical enhancement of PV has been computed for a span of PCM liquification
219 temperature and deepness of PCM box. The results (Fig. 12) suggest that as the temperature for
220 liquification increases from 291 K to 293 K, 295 K, 297 K, 299 K and 301 K, the electrical
221 enhancement period elevates from 6.5 h, 7.3 h, 8.2 h, 9.3 h, 10.7 h and 12.3 h respectively for
222 5 cm deep PCM box. The reason can be explained as follows. The lesser temperature of
223 liquification helps the photovoltaic to operate at lesser temperature which leads to decrement
224 in the losses to surroundings and, consequently, increment in the rate of heat collection by phase
225 change material and increase in the speed of liquification and, thus, drops the period of electrical
226 enhancement.

227 **6. Conclusions**

228 The study aims at finding the period of PV electrical enhancement, electricity generation,
229 electrical efficiency and increase in power achieved using PCM for a span of wind speed, angle
230 of approach of wind, surrounding temperature and PCM liquification temperature. Results
231 suggest that

- 232 (i) As wind speed drops from 6 m/s to 5 m/s, 4 m/s, 3 m/s, 2 m/s, 1 m/s and 0.2 m/s, the
233 electrical enhancement period decreases from 9.1 h to 8.8 h, 8.5 h, 8.0 h, 7.5 h, 6.9 h and
234 6.4 h respectively for 5 cm deep PCM box.
- 235 (ii) As the angle of approach of wind decreases from 75° to 60°, 45°, 30°, 15° and 0°, the
236 electrical enhancement period increases from 7.0 h to 7.6 h, 8.0 h, 8.3 h, 8.5 h and 8.6 h.
- 237 (iii) As the surroundings temperature increases from 289 K to 291 K, 293 K, 295 K, 297 K
238 and 299 K, the electrical enhancement period drops from 12.6 h to 10.9 h, 9.6h, 8.6 h, 7.7
239 h and 7.1 h.
- 240 (iv) As the temperature for liquification increases from 291 K to 293 K, 295 K, 297 K, 299 K
241 and 301 K, the electrical enhancement period elevates from 6.5 h, 7.3 h, 8.2 h, 9.3 h, 10.7
242 h and 12.3 h.

243 Acknowledgment

244 Funding from EPSRC-DST funded Reliable and Efficient System for Community Energy
245 Solution - RESCUES project (EP/K03619X/1) and UKIERI-DST2016-17-0089 project to the
246 University of Exeter and Indian Institute of Technology, Madras is greatly acknowledged. The
247 University of Portsmouth has received funding from the Interreg 2 Seas programme 2014-2020
248 co-funded by the European Regional Development Fund under subsidy contract No 2S04-004.

249 References

250 Arici M., Bilgin F., Nizetic S., Papadopoulos A.M., 2018. *Journal of Cleaner Production* 189,
251 738-745.

252 Atkin P., Farid M.M., 2015. *Solar Energy* 114, 217–228.

253 Baygi S.R.M., Sadrameli S.M., 2018. *Thermal Science and Engineering Progress* 5, 405–411.

254 Benlekkam M.L., Nehari D., Madani H.I., 2018. *International Journal of Heat and Technology*
255 36 (3), 919-926.

256 Biwole P.H., Eclache P., Kuznik F., 2013. *Energy and Buildings* 62, 59–67.

257 Biwole P.H., Groulx D., Souayfane F., Chiu T., 2018. *International Journal of Thermal Sciences*
258 124, 433-446.

259 Brano V.L., Ciulla G., Piacentino A., Cardona F., 2014. *Renewable Energy* 68, 181–193.

260 Browne M.C., Lawlor K., Kelly A., Norton B., McCormack S.J., 2015. *Energy Procedia* 70,
261 163–171.

262 Browne M.C., Norton B., McCormack S.J., 2016. *Solar Energy* 133, 533–548.

263 Emam M., Ahmed A., 2018. *Energy Conversion and Management* 158, 298–314.

264 Emam M., Ookawara S., Ahmed M., 2017. *Solar Energy* 150, 229–245

265 Hasan A., McCormack S.J., Huang M.J., Norton B., 2010. *Solar Energy* 84, 1601–1612.

266 Hasan A., McCormack S.J., Huang M.J., Sarwar J., Norton B., 2015. *Solar Energy* 115, 264–
267 276.

268 Huang M.J., Eames P.C., Norton B., 2004. *International Journal of Heat and Mass Transfer* 47,
269 2715–2733.

270 Huang M.J., Eames P.C., Norton B., 2006. *Solar Energy* 80, 1121–1130.

271 Huang M.J., Eames P.C., Norton B., 2007. *Heat Transfer Engineering* 28, 31-37.

272 Huang M.J., Eames P.C., Norton B., Hewitt N.J., 2011. *Solar Energy Materials & Solar Cells*
273 95, 1598–1603.

274 Indartono Y.S., Suwono A., Pratama F.Y., 2014. *International Journal of Low-Carbon*
275 *Technologies* 0, 1-5.

276 Kamkari B., Groulx D., 2018. *Experimental Thermal and Fluid Science* 97, 94–108.

277 Kant K., Shukla A., Sharma A., Biwole P.H., 2016. *Solar Energy* 140, 151–161.

278 Kaplani E., Kaplanis S., 2014. *Solar Energy* 107, 443–460.

279 Khanna S., Newar S., Sharma V., Reddy K.S., Mallick T.K., 2019. *Energy Conversion and*
280 *Management*. 180, 1185-1195.

281 Khanna S., Sharma V., Singh S., Kedare S.B., 2016. *Applied Thermal Engineering* 103, 323–
282 332.

283 Khanna S., Reddy K.S., Mallick T.K., 2017. *Energy* 133, 887-899.

284 Khanna S., Sharma V., 2015. *Energy* 93, 1788–1803.

285 Khanna S., Sharma V., 2016. *Journal of Solar Energy Engineering* 138, 011010.

286 Khanna, S., Singh, S., Kedare, S.B., 2014. *Energy Procedia* 48, 123–129.

287 Khanna S., Reddy K.S., Mallick T.K., 2018a. *Energy Conversion and Management* 166, 590–
288 601.

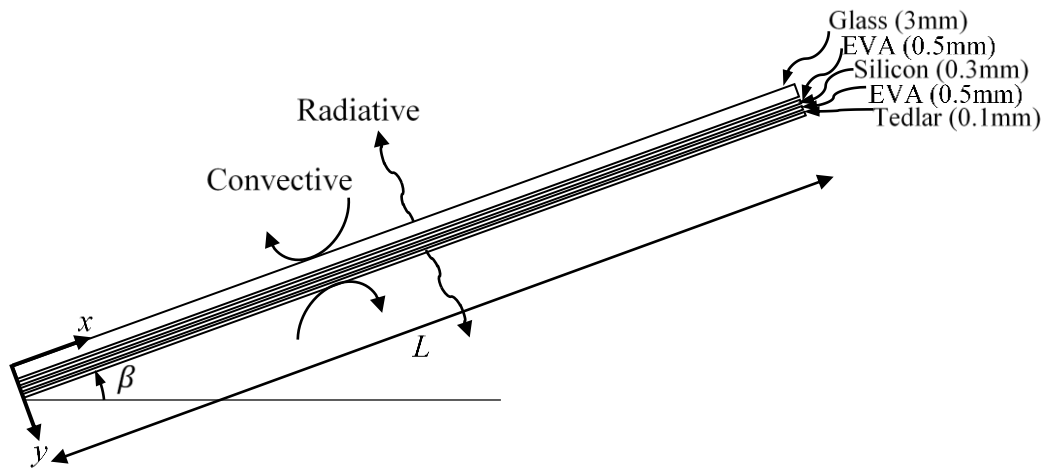
289 Khanna S., Reddy K.S., Mallick T.K., 2018b. *Solar Energy* 174, 593–605.

290 Khanna S., Reddy K.S., Mallick T.K., 2018c. *International Journal of Thermal Sciences*. 130,
291 313-322.

292 Khanna S., Reddy K.S., Mallick T.K., 2018d. *Solar Energy* 163, 591-599.

293 Khanna S., Reddy K.S., Mallick T.K., 2018e. *AIP Conference Proceedings* 2012, 080007.

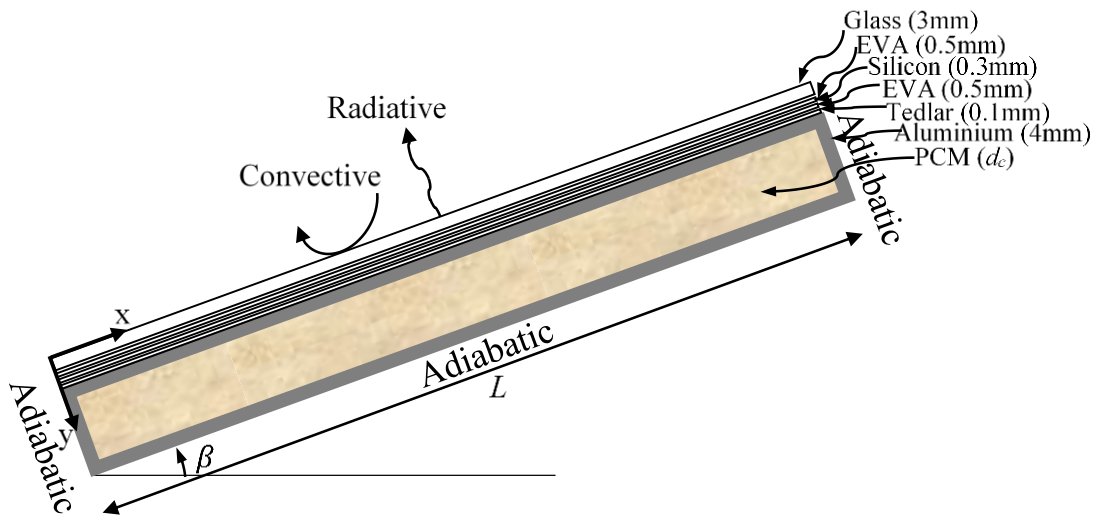
- 294 Khanna S., Sundaram S., Reddy K.S., Mallick T.K., 2017. *Applied Thermal Engineering* 127,
295 559–565.
- 296 Kibria M.A., Saidur R., Al-Sulaiman F.A., Aziz M.M.A., 2016. *Solar Energy* 124, 114–123.
- 297 Lu W., Liu Z., Flor J.F., Wu Y., Yang M., 2018. *Applied Energy* 225, 696-709.
- 298 Ma T., Zhao J., Li Z., 2018. *Applied Energy* 228, 1147-1158.
- 299 Park J., Kim T., Leigh S.B., 2014. *Solar Energy* 105, 561–574.
- 300 Preet S., Bhushan B., Mahajan T., 2017. *Solar Energy* 155, 1104–1120.
- 301 Sathe T. M., Dhoble A.S., 2018. *Journal of Renewable and Sustainable Energy* 10, 043704.
- 302 Sharma S., Micheli L., Chang W., Tahir A., Reddy K.S., Mallick T.K., 2017. *Applied Energy*
303 208, 719–733.
- 304 Sharma V., Khanna S., Nayak J.K., Kedare S.B., 2016. *Energy* 94, 633–653.
- 305 Siyabi I. Al, Khanna S., Mallick T., Sundaram S., 2018a. *AIP Conference Proceedings* 2012,
306 080001.
- 307 Siyabi I. Al, Khanna S., Mallick T., Sundaram S., 2018b. *Energies* 11 (7), 1629.
- 308 Su D., Jia Y., Alva G., Liu L., Fang G., 2017. *Energy Conversion and Management* 131, 79–
309 89.
- 310 Su Y., Zhang Y., Shu L., 2018. *Solar Energy* 159, 777–785.
- 311 Waqas A., Jie J., Xu L., 2017. *Journal of Renewable and Sustainable Energy* 9, 053504.
- 312 Zhang N., Yuan Y., Cao X., Du Y., Zhang Z., Gui Y., 2018. *Advanced Engineering Materials*
313 20, 1700753.



314

315

(a) PV



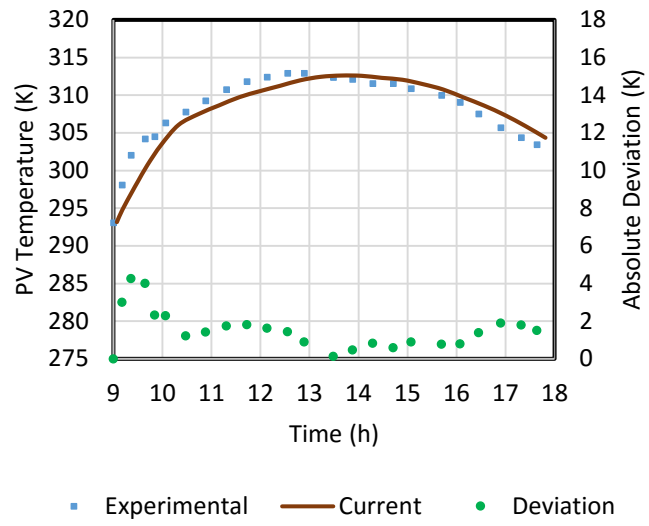
316

317

(b) PV-PCM

318

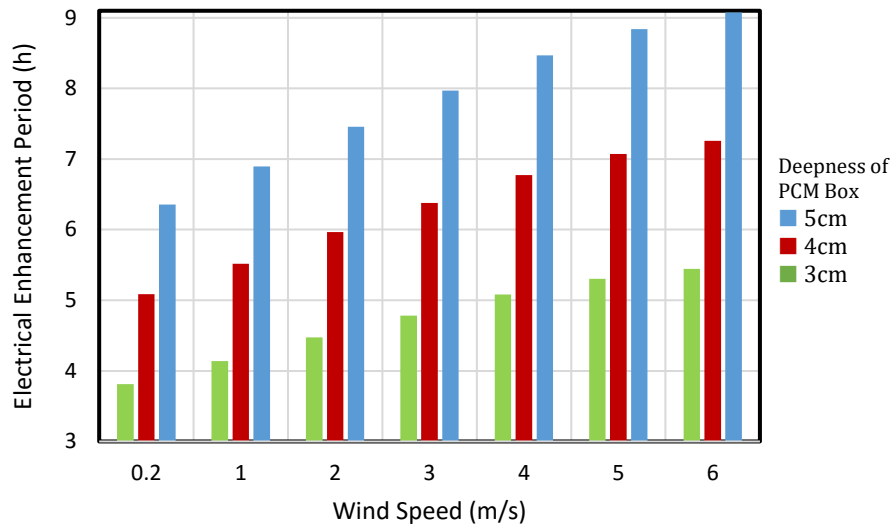
Fig. 1 PV and PV-PCM studied in current work



319

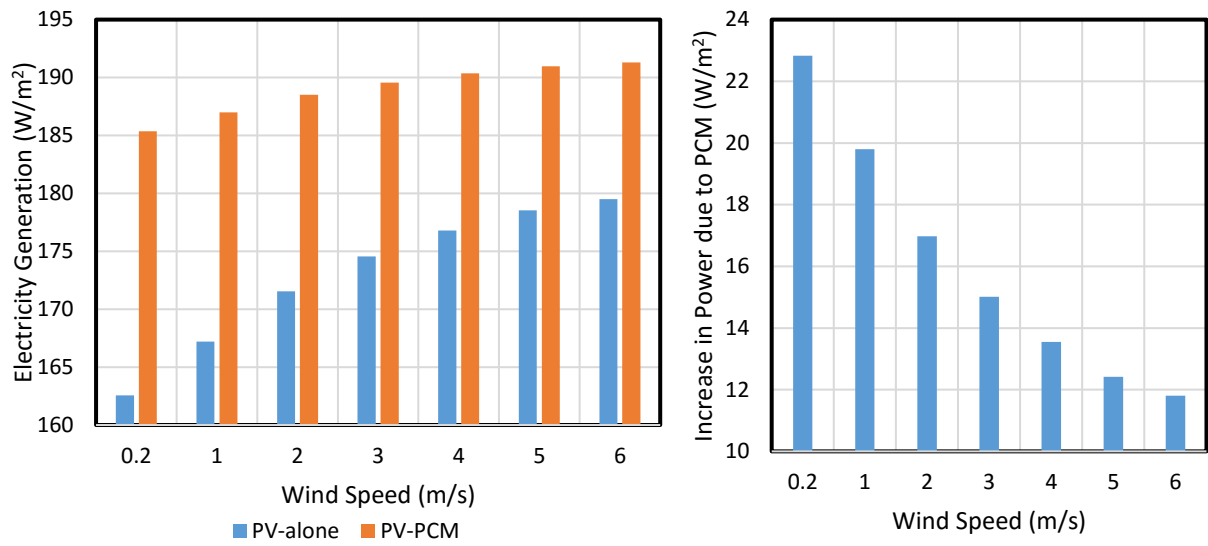
320

Figure 2 Comparison of computed and experimental values (Hasan et al., 2015)



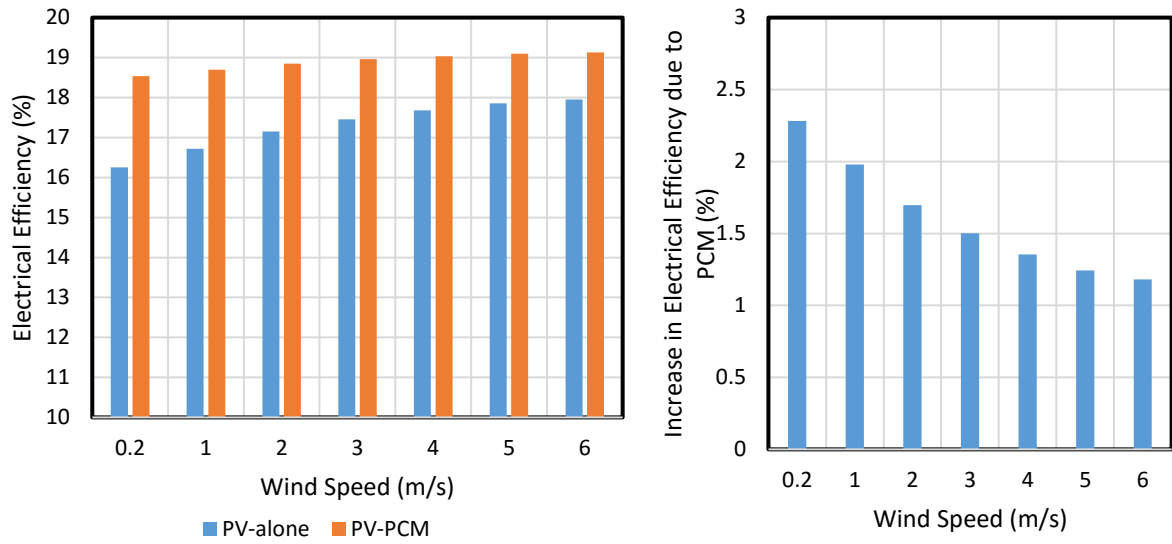
321
 322
 323

Figure 3 Electrical Enhancement Period of PV for a span of wind speed and deepness of PCM box



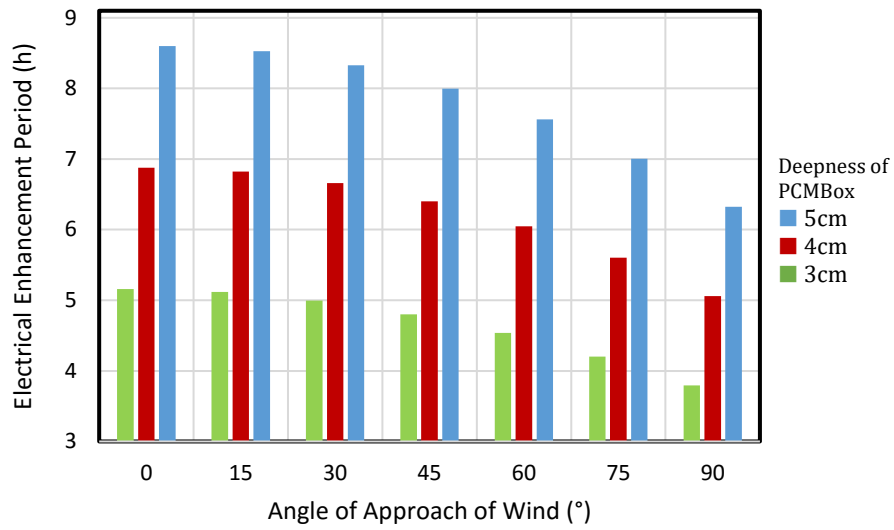
324
 325
 326

Figure 4 Electricity generation and increase in power achieved using PCM for a span of wind speed



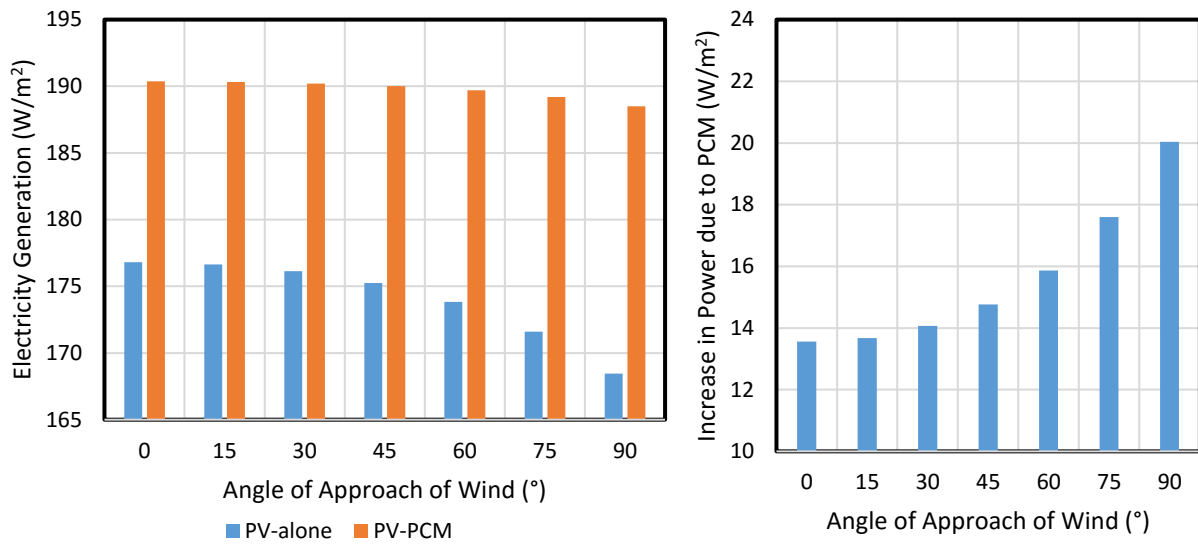
327
 328
 329

Figure 5 Electrical Efficiency and increase in electrical efficiency achieved using PCM for a span of wind speed



330

331 *Figure 6 Electrical Enhancement Period of PV for a span of angle of approach of wind and*
 332 *deepness of PCM box*

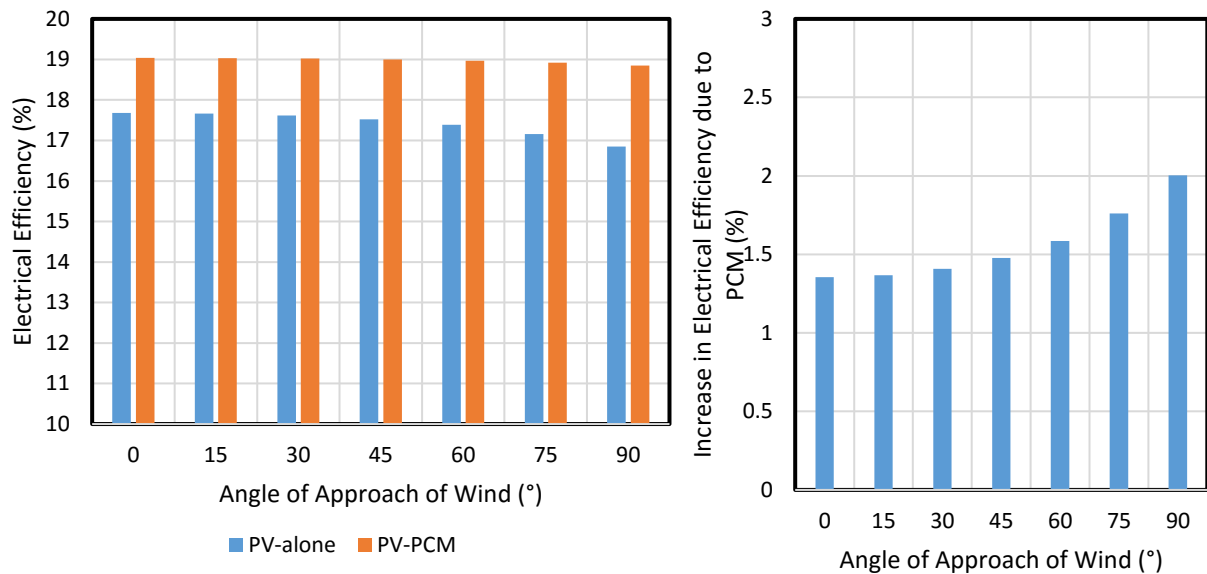


333

334

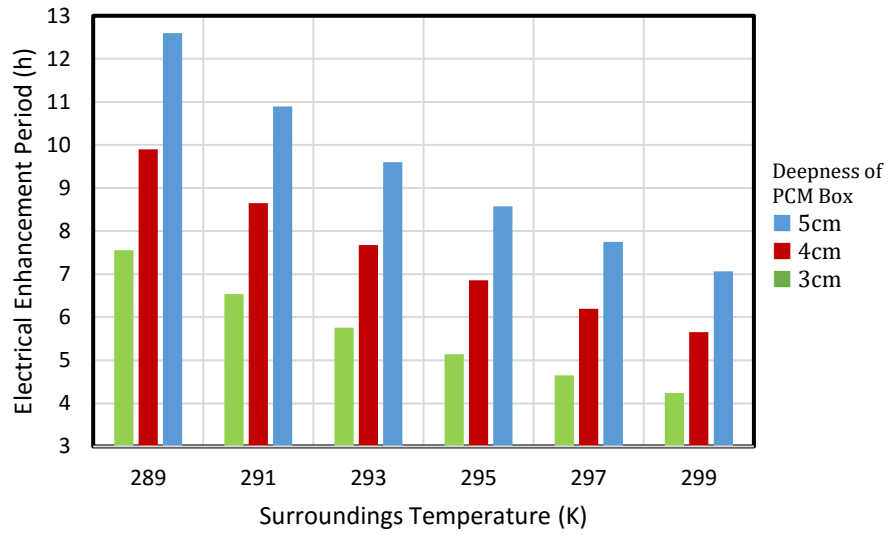
Figure 7 Electricity generation and increase in power achieved using PCM for a span of angle of approach of wind

335



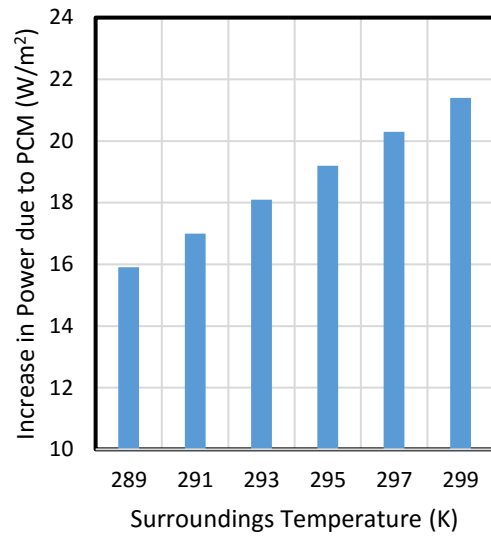
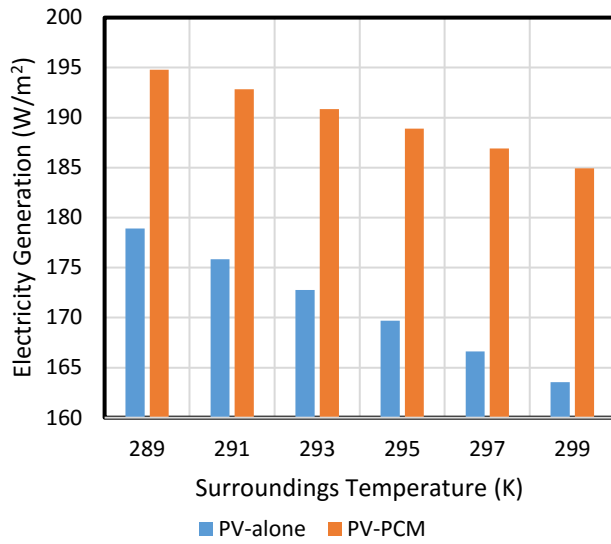
336
 337
 338

Figure 8 Electrical Efficiency and increase in electrical efficiency achieved using PCM for a span of angle of approach of wind



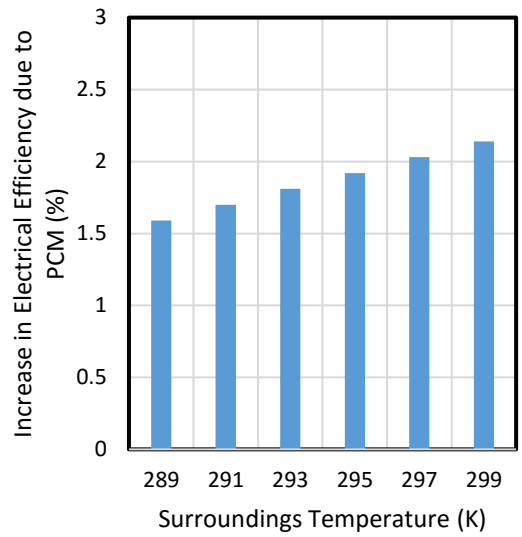
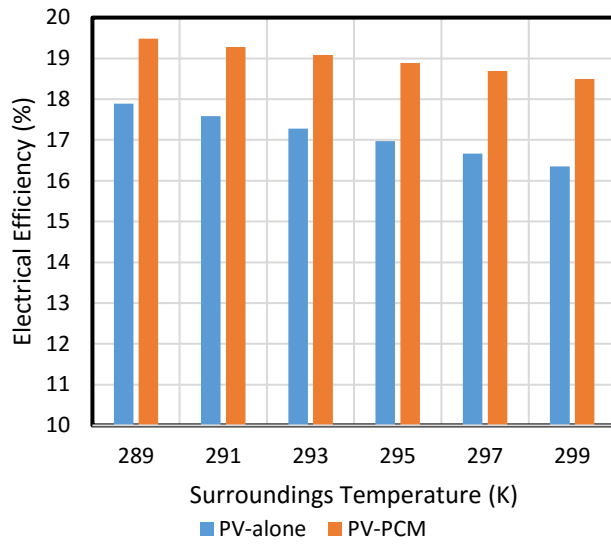
339
 340
 341

Figure 9 Electrical Enhancement Period of PV for a span of surroundings temperature and deepness of PCM box



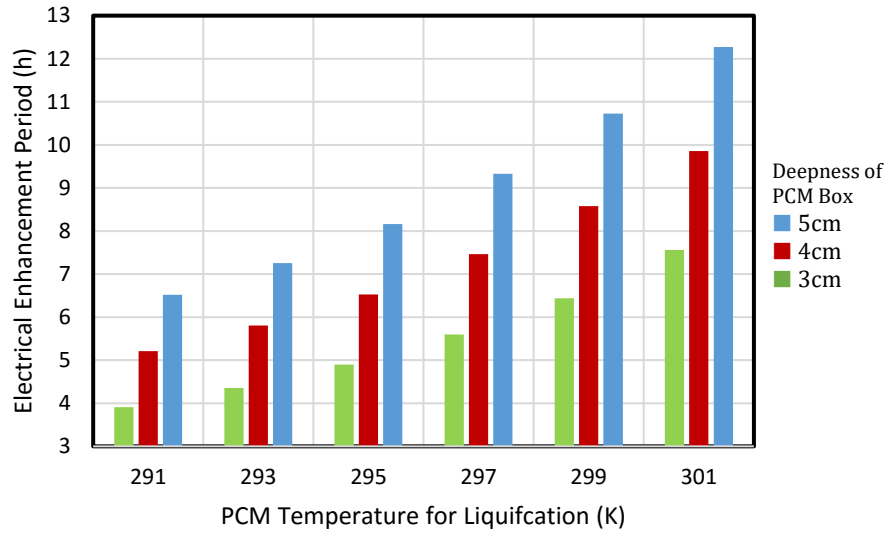
342
343
344

Figure 10 Electricity generation and increase in power achieved using PCM for a span of surroundings temperature



345
346
347

Figure 11 Electrical Efficiency and increase in electrical efficiency achieved using PCM for a span of surroundings temperature



348
 349
 350
 351
 352

Figure 12 Electrical enhancement period of PV for a span of PCM liquifcation temperature and deepness of PCM box